Environment Protection Engineering

Vol. 50 2024 No. 4

DOI: 10.37190/epe240409

PENGFEI SUN (ORCID: 0009-0004-8161-3446)[1]
WENRUI ZHANG (ORCID: 0000-0002-1831-1865)[1]
YAQING ZHANG (ORCID: 0000-0002-8628-9532)[2]
BINGJUN DONG (ORCID: 0009-0006-0819-5537)[1]
YONGCHAO LEI (ORCID: 0009-0002-0551-3123)[1]
DONGJUAN ZENG (ORCID: 0009-0007-4081-2424)[1]
ZHENGHAO XIN (ORCID: 0009-0002-7373-1616)[1]
SHENGJIA ZHANG (ORCID: 0009-0003-7313-0391)[1]
PENG LIANG (ORCID: 0000-0003-2808-865X)[2]

ADSORPTION AND PHOTOCATALYTIC PROPERTIES OF TOLUENE AND RHODAMINE B OVER TiO_2-ZSM-5/CERAMIC FIBER COMPOSITE

TiO_2-ZSM-5/ceramic fiber composite was successfully prepared for the first time by impregnation and applied to remove toluene in the atmosphere and RhB in wastewater. Optional values for TiO_2 loading and calcination temperature were discussed. The composites were characterized by XRD, SEM, TEM, UV-vis and N_2 adsorption-desorption. The results showed that TiO_2 loading amount affects the crystal formation, distribution, pore size and adsorption capacity for pollutants, which in turn determines the adsorption performance and photocatalytic activity of the composite. Composites calcined at 550 °C with 12.7 wt. % TiO_2 loading can degrade toluene and RhB most effectively, with the maximum degradation rates of 39.99% and 92.70%, respectively. In addition, materials have been proven to have high degradation stability being recycled 4 times. The TiO_2-ZSM-5/ceramic fiber prepared in this study can degrade atmospheric and industrial wastewater pollutants. Therefore, TiO_2-ZSM-5/ceramic fiber has high comprehensive practical value in the field of environmental pollutant removal.

[1]College of Safety and Environmental Engineering, Shandong University of Science and Technology, Qingdao, Shandong 266590, China, corresponding author W. Zhang, email address: wenrui.mao@163.com

[2]College of Chemical and Biological Engineering, Shandong University of Science and Technology, Qingdao, Shandong 266590, China.

1. INTRODUCTION

With the rapid development of society and science and technology, environmental pollution has become an important problem facing humankind, among which the emission of volatile organic compounds (VOCs) and industrial wastewater are essential factors causing it [1]. Toluene is one of the more common VOCs with toxicity, bioaccumulation, and other properties [2]. Rhodamine B (RhB) is mainly found in industrial dye wastewater and is a Class 3 carcinogen [3]. Excessive emissions of toluene and RhB can significantly harm the environment and human health. The research showed that photocatalytic oxidation is a rapidly developing green technology in the field of pollutant purification [4–7]. In this regard, photocatalyst is the key to photocatalytic oxidation. Under light excitation, electrons leap from the valence band to the conduction band position, allowing them to form photogenerated electrons (e^-) in the conduction band and photogenerated holes (h^+) in the valence band. Through the redox nature of the photogenerated electron–hole pairs, organic pollutants in the environment can be degraded [8].

TiO_2 plays an important role in semiconductor materials owing to its good photocatalytic properties and stability, thus becoming a research hotspot [7, 9]. Rutile, anatase and slate are the three crystalline forms of TiO_2 with different catalytic properties. Among them, suitable band gap energy of anatase (3.2 ev), reasonable complexation rate, and stability of photogenerated electron pairs and holes make TiO_2 photocatalysts possess remarkable photocatalytic performance and photocatalytic efficiency [8, 10, 11]. Studies have shown that the adsorption of electron acceptors on the catalyst surface has a promotive influence on photodegradation in the process of TiO_2 photocatalytic degradation of pollutants [12]. Moreover, suitable photocatalyst carriers can absorb and concentrate organic pollutants to provide a highly concentrated photocatalytic reaction environment for photocatalysis and improve photocatalytic reaction efficiency. Shi et al. [13] prepared TiO_2/activated carbon fibers catalyst through calcination modification for the photocatalytic degradation of methylene blue in wastewater. The results showed that good adhesion properties existed between TiO_2 films and ACF, which improved the adsorption capacity of the photocatalyst for pollutants and optimized the photocatalytic activity. However, the pure ACF carrier is light in weight and brittle in quality which is not convenient for practical use. And this is also a problem with photocatalysts at present. The commonly used powder photocatalysts have small particle sizes and light specific gravity, making them easily dispersed in the air and difficult to recycle and reused, so that difficult to scale up the industrial application of powder photocatalytic materials effectively. The above problems can be solved if the powder photocatalysts are fixed with suitable carriers [14]. Shao et al. [15] loaded anchor dispersed Co nanoparticles on SBA-16 mesoporous molecular sieve coating grown on a 3D-printed ceramic monolith (SBA-16/ceramic). The ceramic carriers exhibited high specific surface area and mechanical strength. Hong et al. [16] prepared a ceramic fiber/g-C_3N_4 photocatalyst for the degradation of RhB. The

solid light permeability of ceramic fibers allows the catalytic components to receive light to decompose organic dyes, overcoming the limitations of photocatalysts in industrial applications. Yadav et al. [17] prepared BiOX-ceramic fiber composite materials, and the combination of the two materials increased the specific surface area of the materials, and the immobilization of the photocatalyst using ceramic fibers as a substrate helped to recover the photocatalyst. Deng et al. [18] loaded precious metal palladium onto ceramic fibers through ultrasonic impregnation for catalytic oxidation of toluene. Ceramic fibers as carriers are beneficial for controlling the dispersion and oxidation state of the metal, significantly improving the catalytic performance for toluene. In addition, ceramic-based carriers have advantages such as acid-alkali and high-temperature resistance, making them ideal carrier material.

In this paper, ZSM-5 zeolite was impregnated in corrugated ceramic fibers as the composite carrier, and TiO_2 was dispersed on the carrier to obtain the composite catalyst. Its photodegradation performance on toluene gas and RhB solution was investigated under visible light and UV light conditions, and the preliminary application study of the composite provided a valuable exploration to promote the practical engineering application of photocatalytic oxidation technology for the treatment of volatile organic compounds.

2. EXPERIMENTAL

Preparation of catalysts. Corrugated ceramic fiber paper was immersed in the ZSM-5 zeolite slurry and repeated to the required loading several times. Then, it was baked at 450 °C in an air atmosphere to obtain a ZSM-5/ceramic fiber composite (ZSM-5/CF). A certain amount of butyl titanate was added to anhydrous ethanol under stirring to mix uniformly to obtain the TiO_2 precursor solution. ZSM-5/CF was immersed in the TiO_2 precursor solution and taken out to dry naturally to constant weight, where the loading of TiO_2 was controlled by the concentration of butyl titanate. After that, it was calcined at different temperatures (350–600 °C) for 2 h under the nitrogen atmosphere and naturally cooled to room temperature to obtain *x* TiO_2-ZSM-5/CF (*x* is TiO_2 loading amount equal to 3.35, 6.67, 12.97, 22.74, and 28.85 wt. %).

Characterization of catalysts. The X-ray diffraction (XRD) data was obtained by a D/max 2500PC automatic powder X-ray diffract meter equipped with Cu K_α radiation at the range of 10–60° with an 8°/min scan rate. The absorbance of the materials was investigated using a UH4150 UV-vis spectrophotometer from Hitachi. The EVO MA 10L/S10 scanning electron microscope (SEM), FEI Tecnai G2 F30 transmission electron microscope (TEM), and the JSM-2100 high-resolution transmission electron microscope (HRTEM) were used to study the sample morphologies. Nitrogen adsorption and desorption isotherms

of the samples were acquired at 77 K by a volumetric adsorption analyzer (ASAP2020, America). The specific surface areas and the pore size distribution were calculated by the Brunauer–Emmett–Teller (BET) and the Barrett–Joyner–Halenda (BJH) methods, respectively.

Evaluation method of photocatalytic activity of composite material. The photocatalytic performance of the composite materials for the gas toluene (800 cm^3/dm^3) was evaluated using the device shown in Fig. 1.

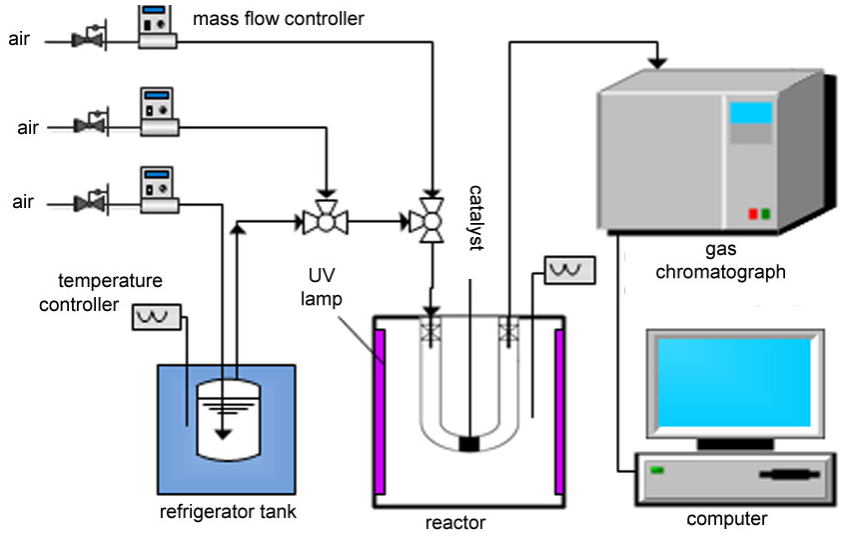

Fig. 1. Schematic diagram of the toluene degradation device

The light source was two ultraviolet lamps with a wavelength of 365 nm and a power of 8 W. The bubbling gas stream passed through the liquid toluene and then merged with the equilibrium gas to obtain the desired concentration of VOCs gas, where the gas flow rates were determined by the space velocity (SV) and saturated vapor pressure of toluene at a specific temperature. The VOCs gas entered the reactor in dark conditions until adsorption saturation; at this point, the saturated adsorption capacity of the materials to toluene was calculated. Then, the light source was turned on and the regeneration gas was passed through for photocatalytic degradation. After 2 hours, the adsorption experiment was performed again to calculate the saturated adsorption capacity of toluene after material regeneration. The concentration of toluene was measured using the online gas chromatograph (GC, SP-6800A) equipped with a flame ionization detector (FID). GC was calibrated by formulating gases of different toluene concentrations before the evaluation of catalyst activity. The breakthrough curve of the sample was plotted according to the change of the outlet concentration with time.

The adsorption of a sample (X, cm^3/g) was calculated by the following equation:

$$X = 10^{-6} q \int_0^t \frac{(C_{in} - C_{out})}{m} dt \tag{1}$$

The conversion of toluene (R_1) was calculated by the following equation:

$$R_1 = \frac{X_1}{X_0} \times 100\% \tag{2}$$

where q is the total gas flow, cm^3/min, t is the time of breakthrough, min, C_{in} and C_{out} are the concentrations of toluene in the inlet and outlet gas, respectively, cm^3/dm^3, m is the amount of composite material, g, X_0 is the saturated adsorption and X_1 is the adsorption after catalysis of the composite material, cm^3/g.

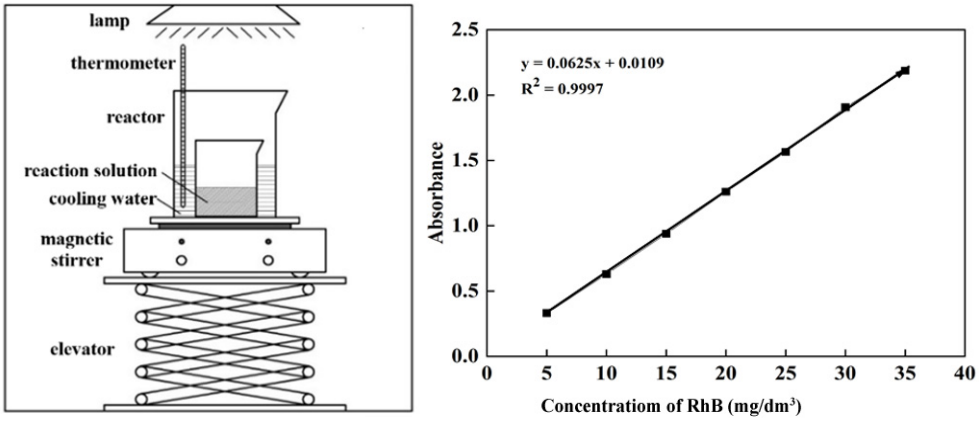

Fig. 2. Schematic diagram of RhB degradation device (a), and calibration curve (b)

The reaction of photocatalytic degradation of RhB was carried out in the experimental setup shown in Fig. 2a, with the light sources of 18 W UV lamp and fluorescent lamp at the main wavelength of 254 nm. The reactor was equipped with 50 cm^3 of 20 mg/dm^3 RhB solution, 50 mg composite material was weighed and added into the reactor. The reaction solution was mixed with a magnetic stirrer; samples were taken every 15 min. After 2 hours, the obtained samples were separated by centrifugation, and the upper clear solution was taken. The solution absorbance was measured using a spectrophotometer, and the absorbance maximum (λ_{max}) of RhB was at 554 nm [19], respectively. Then the concentration of RhB after degradation at different times was determined by the calibration curve. The change in RhB concentration was used to evaluate the catalytic effect of the photocatalyst.

The conversion of RhB (R_2) was calculated by the following formula:

$$R_2 = \frac{C_0 - C_t}{C_0} \times 100\% \tag{3}$$

where C_0 is the initial concentration of the solution and C_t is its concentration at moment t, mg/dm^3.

3. RESULTS AND DISCUSSION

3.1. CHARACTERIZATION RESULTS OF COMPOSITE MATERIALS

Figure 3a shows the XRD patterns of TiO_2-ZSM-5/CF with different TiO_2 content. XRD can be used to analyze the material phase structure information. Samples of c–h exhibited characteristic diffraction peaks of ZSM-5 at 2θ of 23.18°, 23.99° and 24.45°. The peaks at 25.28°, 37.80° and 48.05° correspond to (101), (004) and (105) crystal faces of anatase TiO_2 (JCPD #21-1272), respectively, and the peak at 27.46° corresponds to the rutile phase of TiO_2 (JCPD # 21-1267) [9]. It can be seen that the loading of TiO_2 did not change the crystal form of the ZSM-5 molecular sieve.

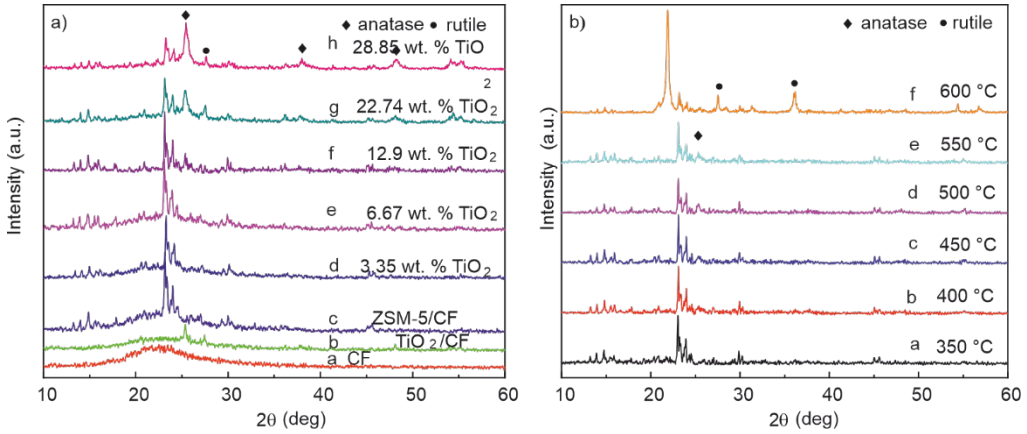

Fig. 3. XRD patterns of: a) TiO_2-ZSM-5/CF with different TiO_2 content, b) 12.97 wt. % TiO_2-ZSM-5/CF at different calcination temperatures; ZSM-5 content 35.38 wt. %

When the TiO_2 loading amount is 3.35 wt. % and 6.67 wt. %, the diffraction peak of TiO_2 is not obvious, indicating that TiO_2 does not form a complete crystal structure, while the characteristic peak of the anatase phase appears when the loading increases to 12.97 wt. %. The rutile phase appeared when the TiO_2 loading increased to 22.74 wt. % and more. As the loading of TiO_2 continues to increase, the characteristic peak of the

anatase phase is more pronounced, indicating that the crystallinity of TiO_2 is enhanced and agglomeration may occur when a certain degree of crystallinity is reached.

Figure 3b shows the XRD patterns of TiO_2-ZSM-5/CF at different calcination temperatures. Upon increasing the calcination temperature to 400 °C, a weak anatase diffraction peak appears at 25.28° indicating that the amorphous TiO_2 begins to transform into the anatase phase. Up to 550 °C, the diffraction peak of anatase increases and becomes sharp pointing to gradual increase of the crystallinity of TiO_2 grains. However, at 600 °C the distinct rutile phase diffraction peaks appear at 27.5° and 36.1° (JCPD #21-1267) [20]. Moreover, a significant diffraction peak of SiO_2 appeared around 21.9° (JCPD #75-0923), showing that the excessive calcination temperature destroys the stability of the molecular sieve and changes its crystal phase.

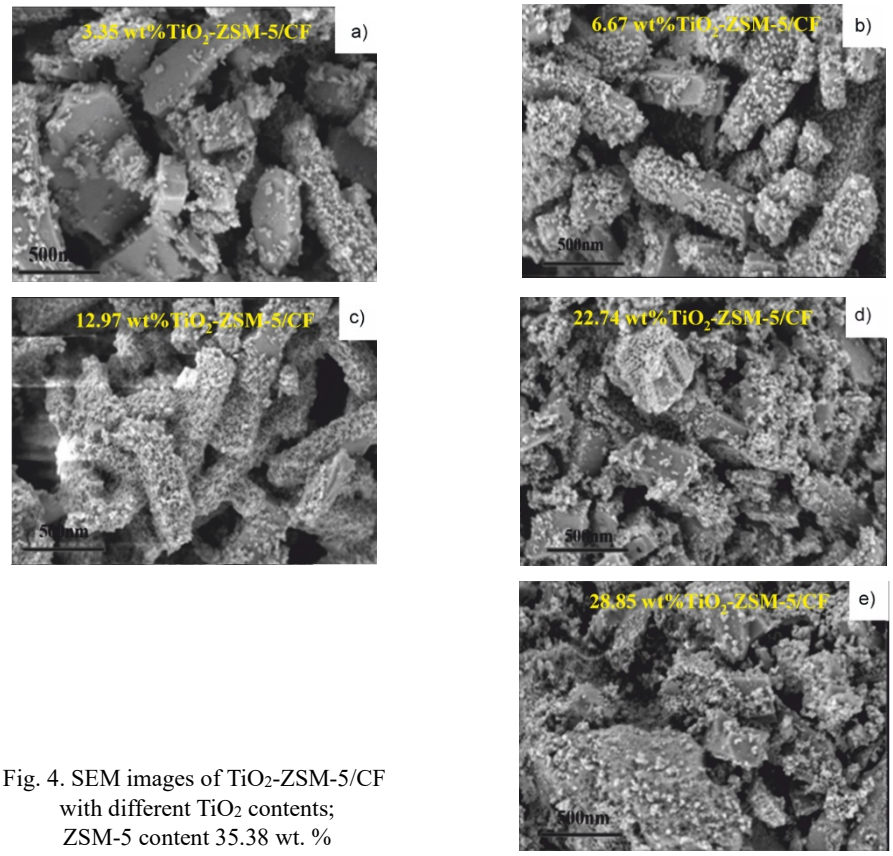

Fig. 4. SEM images of TiO_2-ZSM-5/CF with different TiO_2 contents; ZSM-5 content 35.38 wt. %

Figure 4 shows the SEM images of the composites with different TiO_2 loadings. The surface of the rectangular ZSM-5 molecular sieve is smooth and TiO_2 is loaded onto it in the form of nanoparticles. When the TiO_2 loading was 3.35 wt. %, it was unevenly

distributed on ZSM-5 zeolite. As the TiO_2 loading increased to 12.97 wt. %, TiO_2 particles uniformly distributed and formed a uniform layer on the surface of the zeolite. However, the TiO_2 particles began to agglomerate when the loading of TiO_2 was continued to be added. And the higher the loading of TiO_2 was, the greater the degree of agglomeration. The effect of crystallinity formed by more TiO_2 loading on the structure of the catalyst can also be seen from XRD characterization.

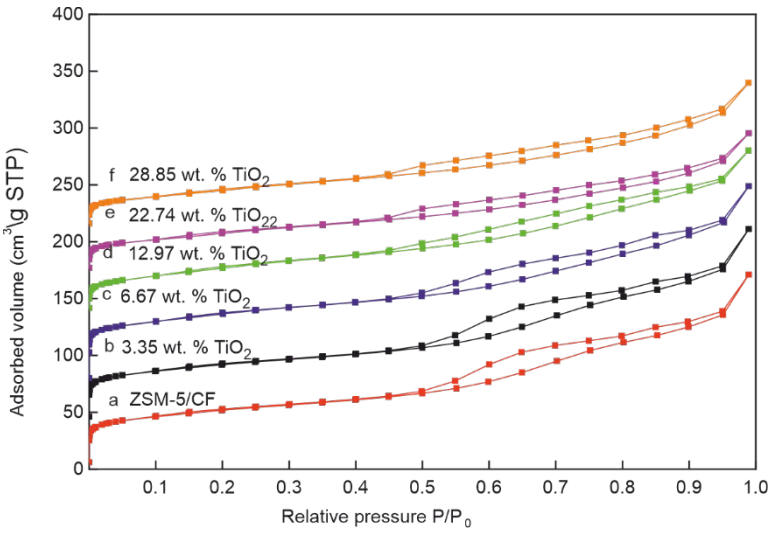

Fig. 5. N_2 adsorption-desorption isotherms of the TiO_2-ZSM-5/CF with different TiO_2 content

Table 1

Structure parameters of TiO_2-ZSM-5/CF with different TiO_2 content

Composite material	Surface area [m^2/g]	Total pore volume [m^3/g]	Average pore diameter [nm]
ZSM-5/CF	1075	0.37	0.56
3.35 wt. % TiO_2-ZSM-5/CF	206	0.19	0.68
6.67 wt. % TiO_2-ZSM-5/CF	210	0.20	0.69
12.97 wt. % TiO_2-ZSM-5/CF	223	0.21	0.72
22.74 wt. % TiO_2-ZSM-5/CF	230	0.23	0.73
28.85 wt. % TiO_2-ZSM-5/CF	238	0.24	0.75

Figure 5 shows the N_2 adsorption-desorption isotherms of TiO_2-ZSM-5/CF with different TiO_2 content. It can be seen that the curves show a rapid increase in the low relative pressure zone, indicating that the composites are rich in microporous structure mainly provided by zeolite. Obvious H3 hysteresis loops in the high relative pressure region of 0.5–1.0 show that the composites contain mesoporous structures, which were mainly due to the slit holes formed by the deposition of molecular sieves and TiO_2. This result

is consistent with the SEM. The pore size distribution of the samples is dispersed from the hysteresis loop in the high pressure region. The specific surface areas of the samples were significantly smaller than that of ZSM-5/CF, as TiO_2 filled a portion of the pores. When TiO_2 load content was increased, the specific surface area, pore diameter and pore volume also increased (Table 1). The microporous structure of the composite material provides a specific surface area of 70% or more, which is favorable for the adsorption of VOCs on the surface.

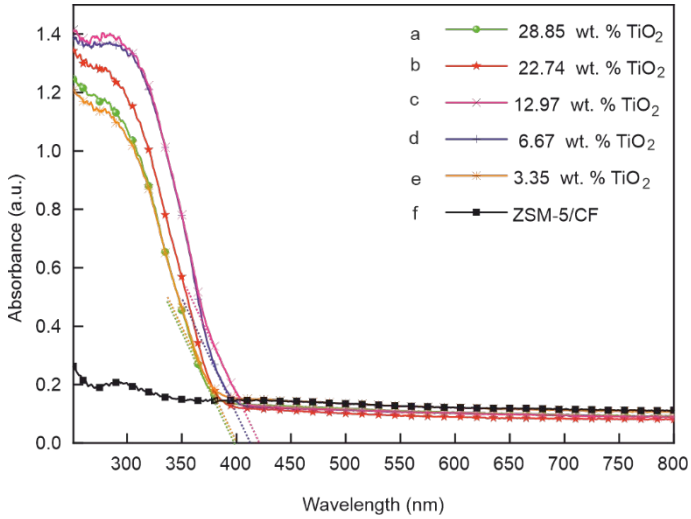

Fig. 6. UV-vis absorption spectra of the TiO_2-ZSM-5/CF with different TiO_2 content

Figure 6 shows the UV-vis absorption spectrum of composite with different TiO_2 loadings. Through UV-vis absorption spectra, the light absorption ability and wavelength of light absorption of composite materials can be examined. Pure ZSM-5/CF has no absorption capacity for ultraviolet light ($\lambda < 400$ nm). With the increasing of TiO_2 content, the ultraviolet light absorption of the composite materials first increased and then decreased. When the loading was 12.97 wt. %, TiO_2 has the highest absorption and utilization rate of ultraviolet light. This is beneficial for the photocatalytic degradation of toluene and RhB. When the loading was continuously increased, the absorbance of the samples gradually decreased. Excessive TiO_2 loading would agglomerate on the zeolite surface, resulting in a decrease in the effective specific surface area that can absorb ultraviolet light. Moreover, the loading of 12.97% TiO_2-ZSM-5/CF has the smallest energy bandwidth among all samples by transforming the Kubelka–Munk function

$$(\alpha h\nu)^2 = A\left(h\nu - E_g\right) \tag{4}$$

where α is the absorption coefficient, h the Planck's constant, ν light frequency, E_g the bandgap energy, and A is a constant.

A successful loading of the appropriate proportion of TiO_2 significantly reduced the band gap of the carrier ZSM-5/CF, which is conducive to the improvement of its electron-hole pairs separation efficiency and the lifetime of photogenerated carriers. Combined with the above characterization and activity evaluation results, the best effect TiO_2 loading of 12.97 wt. % of the composite material was selected to be characterized by TEM, as shown in Fig. 7 (a, b, and c). TiO_2 is mainly deposited on the outer surface of strip shaped ZSM-5 with a thickness of 20 nm, with good contact and uniform dispersion. The HR-TEM image (Fig. 7d) shows the fine crystalline structure with an average d-spacing value of 0.35 nm, corresponding to the (101) plane of the anatase phase as observed in the XRD pattern.

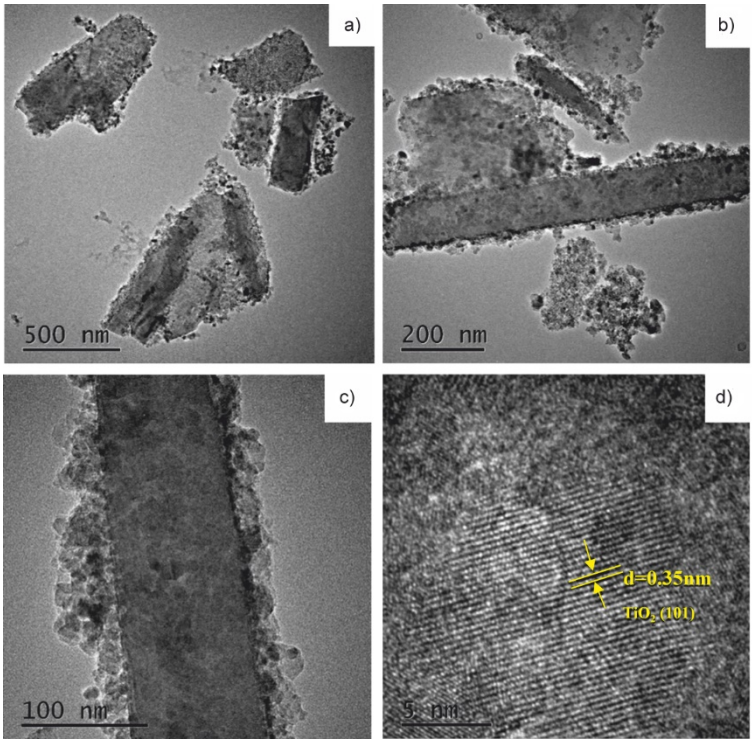

Fig. 7. TEM (a, b, c) and HR-TEM (d) images of 12.97 wt. % TiO_2-ZSM-5/CF

3.2. PHOTOCATALYTIC DEGRADATION PROPERTIES OF COMPOSITE MATERIALS

Figure 8a shows the adsorption and photocatalytic performance of TiO_2-ZSM-5/CF with different TiO_2 contents on toluene. The saturation adsorption capacity of TiO_2--ZSM-5/CF on toluene decreased with the increase of TiO_2 loading, consistent with the

results of the N_2 adsorption-desorption isotherm. After photocatalytic degradation of toluene, the saturation adsorption capacity of the composites on toluene increased and then decreased with the loading increase. When the TiO_2 loading is low, the crystallinity is poor and the UV light absorbance is insufficient, resulting in low photoactivity. With the increase of TiO_2 loading, the crystallinity increased and the dispersion becomes uniform. When the loading amount of TiO_2 reaches 12.97 wt. %, the dispersion degree is the best and the photocatalytic conversion effect is highest (39.99%). However, when the loading is increased continuously, TiO_2 will agglomerate on the surface of ZSM-5 and the UV light absorbance becomes poor, leading to lower photocatalytic degradation. The results indicated that TiO_2 loading amount is an important factor in the photocatalytic conversion effect.

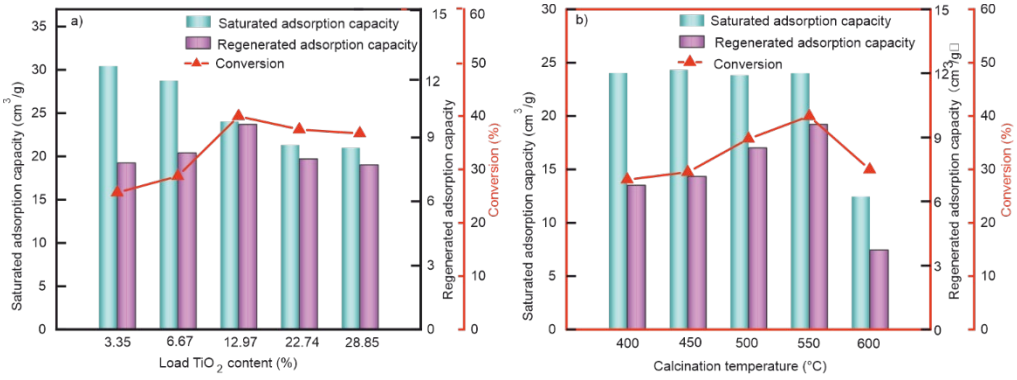

Fig. 8. Adsorption and photocatalytic properties of TiO_2-ZSM-5/CF on toluene with: a) different TiO_2 content at 550 °C, b) different calcination temperatures at 12.97 wt. % of TiO_2-ZSM-5/CF illumination duration 2 h, SV 3500 $cm^3/(h \cdot g)$; VOCs 800 cm^3/dm^3

The saturation adsorption capacity of the composites was unchanged at the calcination temperatures from 400 °C to 550 °C, and the regenerative saturation adsorption capacity and degradation rate gradually increased (Fig. 8b). However, when the calcination temperature was increased to 600 °C, the saturation adsorption capacity, regenerative saturated adsorption capacity and degradation rate decreased significantly. XRD showed that the anatase phase of TiO_2 was weak at low calcination temperature. When the calcination temperature was increased to 550 °C, the increase of the anatase phase promoted the photocatalytic activity of TiO_2. When the calcination temperature was raised to 600 °C, the TiO_2 phase was transformed from anatase to rutile. At this time, the high temperature led to the increase in the particle size of the nano-powder and a small amount of agglomeration [21], which led to the decrease in the photocatalytic activity.

The degradation efficiency of RhB shows a trend of first increasing and then decreasing after 120 minutes of illumination with TiO_2 doping increase (Fig. 9a). The best photocatalytic degradation rate of 92.70% was achieved when the TiO_2 loading was

12.97 wt. %. As the calcination temperature increased, the degradation rate increased first and then decreased (Fig. 9b). The highest conversion was 93.10% at 550 °C, which is consistent with the toluene degradation results. The above indicated that TiO_2-ZSM--5/CF composite has the highest efficiency in degrading toluene and RhB at the TiO_2 loading of 12.97 wt. % and calcination temperature of 550 °C.

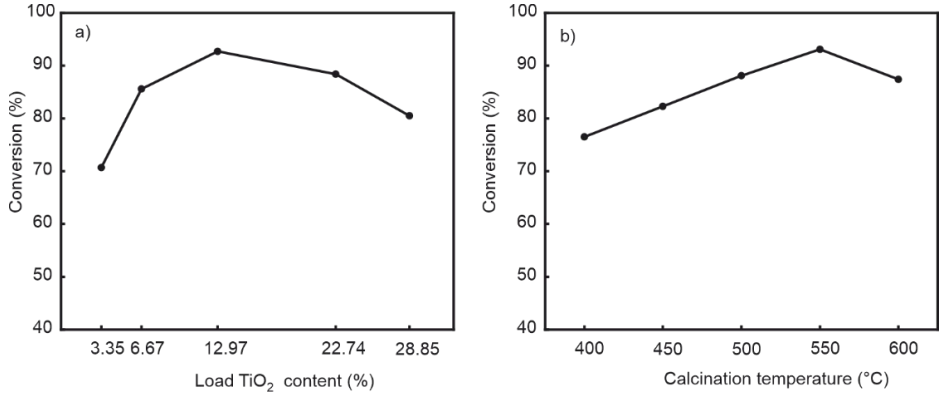

Fig. 9. Degradation properties of composites on RhB depending on:
a) TiO_2 contents, b) calcination temperature

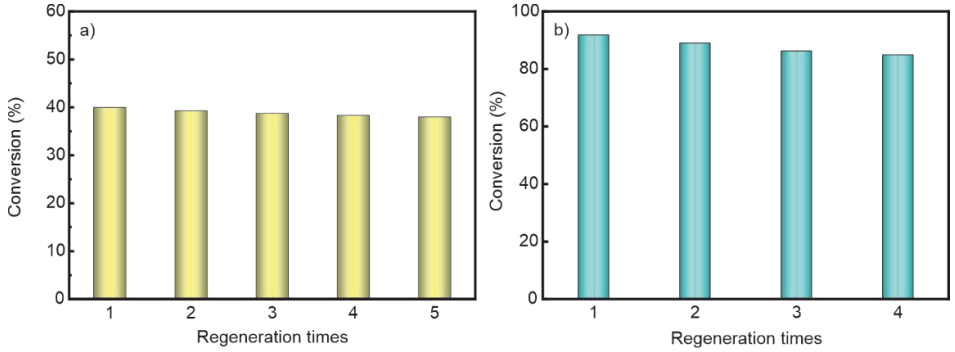

Fig. 10. Recycling stability of TiO_2-ZSM-5/CF for degradation of:
a) toluene, b) RhB; illumination duration 2 h, SV 3500 $cm^3/(h \cdot g)$

The recycling performance test was performed on TiO_2-ZSM-5/CF composites with TiO_2 loading of 12.97 wt. % and calcination temperature of 550 °C. The regeneration conditions were 2 h of UV light and 3500 $cm^3/(h \cdot g)$ of space velocity. The TiO_2-ZSM-5/CF composites were reused four times and the photocatalytic degradation efficiency of toluene and RhB remained above 38% and 88%, respectively (Fig. 10). During the experiments, the degradation rate decreased slightly due to the slight change in sample morphology caused by each centrifugal separation and the loss of doped TiO_2. However, the

degradation rate remained basically unchanged in four repetitive experiments, and it can be seen that the composite has good stability and a high application value.

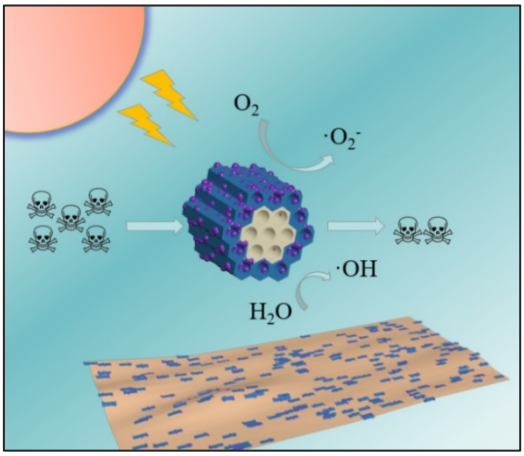

Fig. 11. A possible removal mechanism on TiO_2-ZSM-5/CF

Based on the results of this experiment and relevant literature research [22], explore the potential pathways and mechanisms of removing organic pollutants in the TiO_2--ZSM-5/CF composite material prepared in this experiment (Fig. 11). Toluene and RhB were adsorbed onto ZSM-5/CF with a rich microporous structure and large specific surface area. Then, TiO_2 is excited to acquire band gap energy under UV irradiation. The electrons jump from the valence band to the conduction band, and the electron-hole stays in the valence band. When TiO_2 loading is 12.97 wt. % and calcined at 550 °C, the TiO_2 distribution is uniform in TiO_2-ZSM-5/CF. The increase of the anatase phase improves the separation efficiency of the electron-hole pairs and the lifetime of the photogenerated carriers. Electrons in the conduction band react with O_2 in the reaction medium (air or water) to form a superoxide anions $(\cdot O_2^-)$, while holes in the valence band can oxidize the pollutant directly or react with H_2O to form a hydroxyl radicals (·OH). Both superoxide anions and and hydroxyl radicals with strong oxidizing properties can interact with toluene and RhB, adsorbing and degrading them and finally achieving the purpose of elimination.

4. CONCLUSIONS

ZSM-5 zeolite was impregnated into corrugated ceramic fibers for the first time to form a carrier with high mechanical strength, and the active component TiO_2 was successfully loaded on its surface. The effects of TiO_2 loading and calcination temperature on the photocatalytic activity were investigated. Results show that the TiO_2 loading and

calcination temperature affect the crystal structure, pore size and active component distribution of TiO_2-ZSM-5/CF, which in turn determine the adsorption performance and photocatalytic activity of the composites. Among them, the TiO_2-ZSM-5/CF prepared at 12.97 wt. % TiO_2 and 550 °C had the best removal performance for toluene and RhB, with removal rates of 39.99% and 92.70%, respectively. The composites showed good stability with the removal and degradation of toluene and RhB remaining above 38% and 88% after regenerating and recycling four times. The catalyst prepared in this work can degrade both gas-phase and liquid-phase organic pollutants, which is highly valuable for comprehensive industrial applications.

ACKNOWLEDGEMENTS

This work was supported by the National Natural Science Foundation of China (grant numbers 42107284, 22208195, and 22078177).

REFERENCES

[1] HE C., CHENG J., ZHANG X., DOUTHWAITE M., PATTISSON S., HAO Z., *Recent advances in the catalytic oxidation of volatile organic compounds: a review based on pollutant sorts and sources*, Chem. Rev. 2019, 119 (7), 4471–4568. DOI: 10.1021/acs.chemrev.8b00408.

[2] ZHAO Q., ZHENG Y., SONG C., LIU Q., JI N., MA D., LU X., *Novel monolithic catalysts derived from in-situ decoration of Co_3O_4 and hierarchical Co_3O_4@ MnO_x on Ni foam for VOC oxidation*, Appl. Catal. B, 2020, 265, 118552. DOI: 10.1016/j.apcatb.2019.118552.

[3] MOHAMMAD-REZAEI R., KHALILZADEH B., RAHIMI F., REZAEE P., ARAB S.-S., DERAKHSHANKHAH H., JAYMAND M., *Simultaneous removal of cationic dyes from simulated industrial wastewater using sulfated alginate microparticles*, J. Mol. Liq. 2022, 363, 119880. DOI: 10.1016/j.molliq.2022.119880.

[4] SAEED M., MUNEER M., HAQ A.U., AKRAM N.J.E.S., *Photocatalysis. An effective tool for photodegradation of dyes. A review*, Environ. Sci. Pollut., 2022, 1–19. DOI: 10.1007/s11356-021-16389-7.

[5] GUO W., GUO T., ZHANG Y., YIN L., DAI Y., *Progress on simultaneous photocatalytic degradation of pollutants and production of clean energy. A review*, Chemosphere, 2023, 139486. DOI: 10.1016 /j.chemosphere.2023.139486.

[6] GUO D., FENG D., ZHANG Y., ZHANG Y., ZHAO Y., ZHOU Z., SUN J., QUAN C., CHANG G., SUN S., *Carbon material–TiO_2 for photocatalytic reduction of CO_2 and degradation of VOCs. A critical review*, Fuel Proc. Tech., 2022, 231, 107261. DOI: 10.1016/j.fuproc.2022.107261.

[7] LU M., YANG W., YU C., LIU Q., YE D.J., *Plasma-catalytic oxidation of toluene on Ag modified FeO_x/SBA-15*, Aeros. Air Qual. Res., 2020, 20 (1), 193–202. DOI: 10.4209/aaqr.2019.09.0467.

[8] GUO Q., ZHOU C., MA Z., YANG X., *Fundamentals of TiO_2 photocatalysis: concepts, mechanisms, and challenges*, Adv. Mater., 2019, 31 (50), 1901997. DOI: 10.1002/adma.201901997.

[9] LIANG P., WEI A., ZHANG Y., WU J., ZHANG X., LI S., *Immobilisation of TiO_2 films on activated carbon fibres by a hydrothermal method for photocatalytic degradation of toluene*, Micro Nano Lett., 2016, 11 (9), 539–544. DOI: 10.1049/mnl.2016.0171.

[10] TIAN J., TUO B., WANG J., TANG Y., NIE G., YANG Y., *Preparation of different crystal types TiO_2 materials and its photodegradation performance in Congo Red wastewater*, Phase Trans., 2022, 95 (10), 707–725. DOI: 10.1080/01411594.2022.2107927.

[11] CHO Y., KIM S., PARK B., LEE C.-L., KIM J.K., LEE K.-S., CHOI I.Y., KIM J.K., ZHANG K., OH S.H., *Multiple heterojunction in single titanium dioxide nanoparticles for novel metal-free photocatalysis*, Nano Lett., 2018, 18 (7), 4257–4262. DOI: 10.1021/acs.nanolett.8b01245.

[12] ZHU X., WANG D., HUI S., *Research progress of adsorption and photocatalysis of formaldehyde on TiO_2/AC*, Ads. Sci. Technol., 2021, 1–16. DOI: 10.1155/2021/8790974.

[13] SHI J.-W., CUI H.-J., CHEN J.-W., FU M.-L., XU B., LUO H.-Y., YE Z.L., *TiO_2/activated carbon fibers photocatalyst: Effects of coating procedures on the microstructure, adhesion property, and photocatalytic ability*, J. Colloid Interf. Sci., 2012, 388 (1), 201–208. DOI: 10.1016/j.jcis.2012.08.038.

[14] WANG J., SUN S., PAN L., XU Z., DING H., LI W., *Preparation and properties of $CaCO_3$-supported nano-TiO_2 composite with improved photocatalytic performance*, Mater., 2019, 12 (20), 3369. DOI: 10.3390/ma12203369.

[15] SHAO Y., YAN Y., WANG J., JIN Q., XU H., ZHANG X., *Co/SBA-16 coating supported on a 3D-printed ceramic monolith for peroxymonosulfate-activated degradation of Levofloxacin*, J. Coll. Interf. Sci., 2023, 643, 137–150. DOI: 10.1016/j.jcis.2023.03.112.

[16] HONG J., KIM J., SELVARAJ R., KIM Y., *Chemistry, Immobilization of visible-light-driven photocatalyst g-C_3N_4 on ceramic fiber for degradation of organic dye*, Toxic. Environ. Chem., 2021, 103 (1), 18–36. DOI: 10.1080/02772248.2021.1879083.

[17] YADAV M., GARG S., CHANDRA A., HERNADI K., *Immobilization of green BiOX (X= Cl, Br and I) photocatalysts on ceramic fibers for enhanced photocatalytic degradation of recalcitrant organic pollutants and efficient regeneration process*, Cer. Int., 2019, 45 (14), 17715–17722. DOI: 10.1016/j.ceramint. 2019.05.340.

[18] DENG H., KANG S., WANG C., HE H., ZHANG C., *Palladium supported on low-surface-area fiber-based materials for catalytic oxidation of volatile organic compounds*, Chem. Eng. J., 2018, 348, 361–369. DOI: 10.1016/j.cej.2018.04.184.

[19] BAI X., DU Y., XUE W., HU X., FAN J., LI J., LIU E., *Enhancement of the photocatalytic synchronous removal of Cr(VI) and RhB over RP-modified flower-like SnS_2*, Nanosc. Adv., 2020, 2 (9), 4220–4228. DOI: 10.1039/d0na00489h.

[20] ZHOU Y., LI M., ZHONG X., ZHU Z., DENG P., LIU H., *Hydrophobic composite coatings with photocatalytic self-cleaning properties by micro/nanoparticles mixed with fluorocarbon resin*, Cer. Int., 2015, 41 (4), 5341–5347. DOI: 10.1016/j.ceramint.2014.12.090.

[21] ZHANG Q., LI C., *Pure anatase phase titanium dioxide films prepared by mist chemical vapor deposition*, Nanomater., 2018, 8 (10), 827. DOI: 10.1016/j.apcatb.2019.118552.

[22] ZHANG W., WANG Y., HAO M., ZHANG H., LIANG P., *Enhanced photocatalytic degradation of organic pollutants under visible light using Ag-modified TiO_2 on activated carbon fibers*, Nano., 2021, 16 (10), 2130009. DOI: 10.1142/s1793292021300097.